Elif Çelenk Kaya*, Afşin Ahmet Kaya, Zeynep Demircioğlu and Orhan Büyükgüngör

Synthesis, spectroscopic characterization, X-ray structure and DFT calculations of Ni(II)bis(3,4 dimethoxybenzoate)bis(nicotinamide) dihydrate

DOI 10.1515/hc-2016-0099
Received June 22, 2016; accepted January 11, 2017; previously published online March 28, 2017

Abstract: A single crystal of Ni(II)bis(3,4 dimethoxybenzoate)bis(nicotinamide) dihydrate, formulated as $C_{30}H_{34}N_4NiO_{12}$ (I), was characterized in the solid state by infra-red (IR), ultra-violet (UV) and single crystal X-ray diffraction analysis at 296 K as mononuclear with a distorted octahedral stereochemistry. The complex consists of a six-coordinate Nickel atom in a distorted octahedral environment constructed from two N atoms and four O atoms and crystallizes in the monoclinic space group *C 2/c* with $a = 27.7680(16)$ Å, $b = 8.5748(3)$ Å, $c = 17.8018(9)$ Å, $\alpha = 90°$, $\beta = 108.154(4)°$, $\gamma = 90°$, $Z = 4$. The molecular structure and geometry was also optimized using the B3LYP density functional theory method employing the 6-31G(d) basis set. The molecular electrostatic potential (MEP), frontier molecular orbitals (FMO) analysis, nonlinear optical properties (NLO) and natural bond analysis (NBO), Mulliken population analyis, natural population analysis (NPA) and Fukui function analysis were also described.

Keywords: density functional theory (DFT); Fukui function analysis; natural bond analysis; natural population analysis; nicotinamide.

Introduction

Nicotinamide and nicotinic acid are two of the most extensively studied pyridine derivatives [1]. The former is a component of the vitamin B complex and of the vital co-enzyme nicotinamide adenine dinucleotide (NAD) [1, 2]. Nicotinamide has been reported to impair learning and memory in mice [3]. The medicinal chemistry of nicotinamide in the treatment of ischemia and reperfusion has developed rapidly in the past few years. Nicotinic acid has a wide-ranging ability to reduce lipid levels, but its clinical uses are restricted due to side effects. Nicotinic acid and nicotinamide moieties are present in niacin, a water-soluble vitamin that reduces concentration of low density lipoprotein cholesterol [4]. Moreover, co-ordination compounds of nicotinic acid, nicotinamide, and their derivatives are known to have antiviral or antibacterial activity [5, 6] and they also selectively affect tumor tissues [7].

In recent decades, metallocomplexes have received much attention as promising compounds for the development of drugs. Different metal ions can modify both magnitude and direction of the pharmacological activity of the initial organic compounds (ligands) as a result of changes in their size, shape, charge density distribution, and redox potentials [8]. It has been reported that chelation causes drastic change in the biological properties of the ligands [9–11]. Much of the toxicity of nickel may be associated with its interference with the physiological processes of manganese, zinc, calcium and magnesium [12]. Various diseases such as myocardial infarction and acute stroke and injuries are associated with altered transport and serum concentrations of nickel [13].

In this paper, we report the molecular and crystal structures of (Ni(II)bis(3,4-dimethoxybenzoate)bis(nicotinamide) dihydrate (Scheme 1). The molecular structure and molecular geometry results were also computed using DFT/B3LYP employing the 6-31G(d) basis set.

Results and discussion

Synthesis

The nickel complex was synthesized as shown in Scheme 1. Details are provided in the experimental section.

Crystal structure

In the title compound, $C_{30}H_{34}N_4NiO_{12}$, the Ni ion is located on a crystallographic inversion center (Figure 1). The

***Corresponding author: Elif Çelenk Kaya,** School of Health, Gümüşhane University, TR-29100, Gümüşhane, Turkey, e-mail: elifcelenk1629@hotmail.com
Afşin Ahmet Kaya: School of Health, Gümüşhane University, TR-29100, Gümüşhane, Turkey
Zeynep Demircioğlu and Orhan Büyükgüngör: Department of Physics, Faculty of Arts and Sciences, Ondokuz Mayıs University, 55139 Kurupelit-Samsun, Turkey

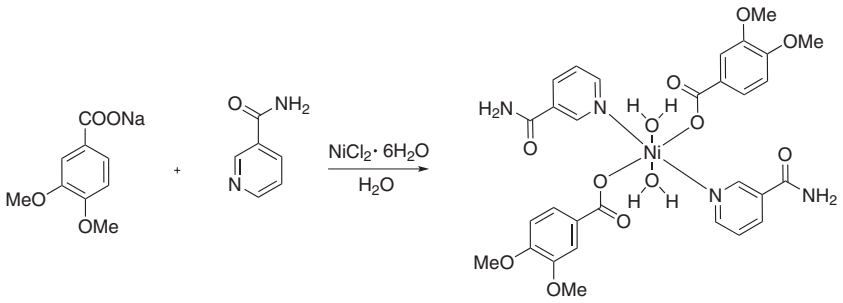

Scheme 1

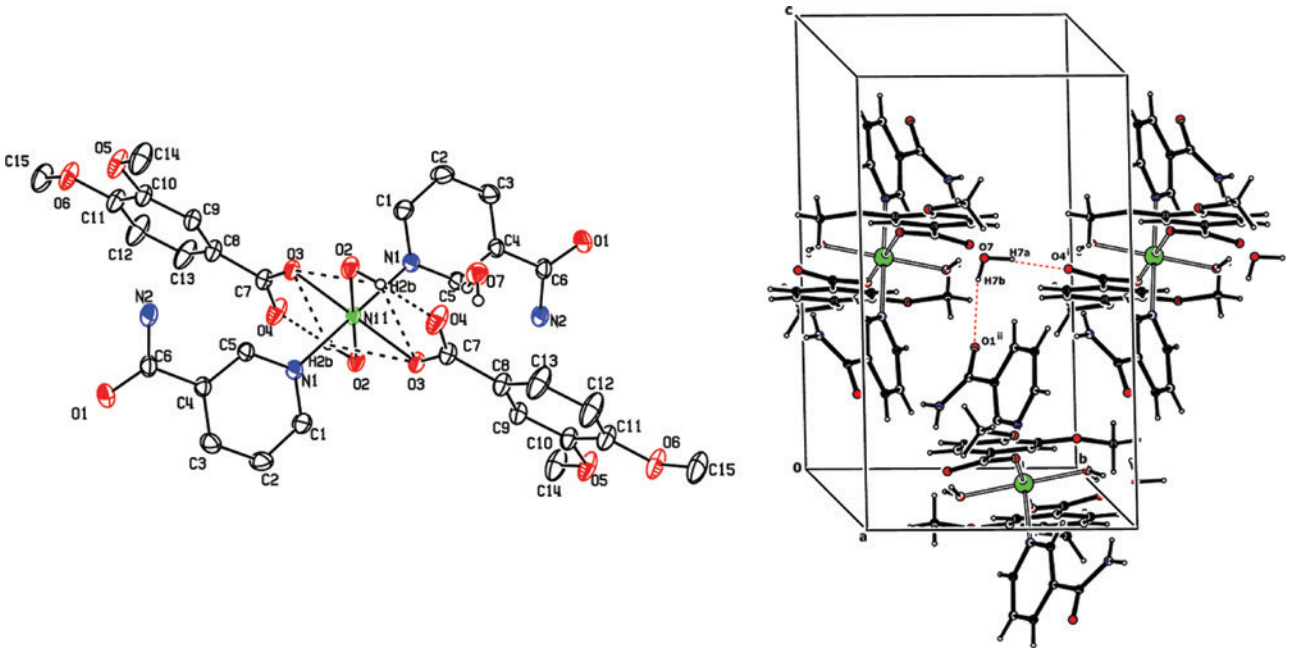

Figure 1 Ortep 3 diagram and crystal packing diagram for the title compound.
For clarity of presentation, the hydrogen atoms are deleted. Black dashed lines show the O-H…O intramolecular bondings. A partial packing diagram with O7-H7a…O4^{i} and O7-H7b…O1^{ii} intermolecular hydrogen bonds are shown as red dashed lines [symmetry code: (i): x, 1+y, z, (ii): 1/2–x, 1/2+y, 1/2-z].

Ni center co-ordinates the two oxygen atoms from two 3,4-dimethoxy benzoate moieties, two nitrogen atoms from two nicotinamide moieties, and two oxygen atoms from a pair of water molecules to form an octahedral geometry. The similar lengths of the bonds Ni-N1 [2.0824(16) Å; 2.0824(16) Å]; Ni-O3 [2.07(14) Å; 2.07(14) Å]; Ni-O2 [2.0605(15) Å; 2.0605(15) Å] indicate a delocalized bonding arrangement, rather than localized single and double bonds. These values are in satisfactory agreement with those reported in the literature [14–16]. The angles N1-Ni-O3, O2-Ni-O3, C1-N1-Ni, C7-O3-Ni angles are 92.20(6)°, 88.48(6)°, 120.91(14)° and 128.89(13)°, respectively.

The O2-H2b…O4 and O2-H2b…O3 intramolecular interactions constitute a pair of bifurcated donor bonds generating two fused rings (Figure 1, Table S2). The p-stacking interactions are not observed in the crystal packing. Despite the interplanar distance being smaller than 4.0 Å, the centroid-centroid distances are bigger than 4.0 Å. The crystal packing of the title compound is mainly stabilized by O7-H7A…O4^{i} [symmetry code (i): x, 1+y, z] and O7-H7B…O1^{ii} [symmetry code (ii): 1/2–x, 1/2+y, 1/2–z] intermolecular hydrogen bondings [17].

Theoretical structure

The neutral molecule in the ground state (charge 0) with spin multiplicity 1 (singlet) was optimized using the spin-restricted hybrid DFT (RB3LYP) method. The molecule was calculated using the density functional theory

(B3LYP) method with 6-31G(d) basis set for C, H, N and O atoms. Electronic transitions were calculated using the time-dependent density functional theory (TD-DFT) formalism and compared with the experimental spectrum. Some structural parameters obtained experimentally and theoretically by B3LYP/ 6-31G(d) are given in Table S3 for comparison. The differences observed between the experimental and calculated parameters are due to a selected theoretical method, basis set and ignored effects, namely the intermolecular interactions and theoretical calculation errors. In addition, the experimental results are for the solid state but the calculated results are for the isolated gaseous phase. In particular, the optimized geometry with B3LYP is more planar than the conformation derived from X-ray diffraction analysis.

Vibrational spectra

In the infra-red (IR) spectrum of the Ni(II) complex the OH absorption bands of aqua ligands are present around 3215 cm^{-1} and correspond to stretching vibrations of water molecules. The complex has a strong band for the C=O stretching. Conjugation between the carbonyl group and amide nitrogen causes small frequency shifts. The strong band observed at 1676 cm^{-1} is assigned to this mode. Pyridine ring vibrations of free nicotinamide at 1515 cm^{-1} are shifted to lower frequencies in the spectrum of the metal complex. The shift is observed around 1412 cm^{-1} approximately, which indicates that the pyridine ring is coordinated. The main difference in the spectrum of 3,4-dimethoxybenzoic acid is that the C=O stretching vibration at 1725 cm^{-1} is shifted to lower frequency in the metal complex. These same modes are supported by the literature data [15]. The absorption bands of the carboxylate groups in the metal complex are observed around 1676 cm^{-1}. The low-intensity bands in a region of 600–400 cm^{-1} are attributed to the M-N and M-O vibrations.

Electronic absorption spectra

The electronic absorption spectra of Ni(II) complex in various solvents (benzene, chloroform, ethanol, DMSO) were calculated at the TD-DFT at B3LYP/631G(d) level for the polarizable continuum model (PCM). The theoretical and experimental absorption wavelengths are given in Table S3. It is known that the $\pi \rightarrow \pi^*$ transition is shifted to a longer wavelength with increasing the solvent polarity and the energy of the π^* orbital is decreased. The related results given in Table S4 are in satisfactory agreement with those described in the literature [14]. Theoretical calculation results indicate that the structure in the gas phase is more stable than the structures in several solvents (DMSO, ethanol, chloroform, benzene) because the calculations in gas phase do not consider intermolecular interactions. The energy gap (ΔE) affects the stability of the molecule and determines its chemical reactivity, kinetic stability, polarizability and chemical reactivity [18]. If the molecule has a large energy gap, it is more stable in regard to its chemical reactivity. Soft regions of a molecule are more polarizable and more reactive than its hard regions. With respect to the results of this report, the title compound shows high polarizability, reactivity and softness.

Frontier molecular orbitals (FMOs)

The highest occupied molecular orbitals (HOMOs) and the lowest unoccupied molecular orbitals (LUMOs) are named as FMOs [19, 20]. The frontier orbital gap helps characterize the chemical reactivity and the kinetic stability of the molecule. A molecule with a small frontier orbital gap is generally associated with a high chemical reactivity, low kinetic stability and is also termed as soft molecule [21].

The distributions of the HOMO and LUMO orbitals computed at the B3LYP/6-31G(d) level for the title molecule are illustrated in Figure 2. The calculated energy values are $E_{HOMO} = -3.944$ eV and $E_{LUMO} = -1.314$ eV. The calculations indicate that the title compound has 108 occupied MOs. While the LUMOs are delocalized on almost a whole molecule, HOMOs are localized on the Ni ion and the nicotinamide group. The title molecule has a narrow HOMO-LUMO gap of 2.595 eV, which implies high kinetic stability and low chemical reactivity [22, 23].

Mulliken electronegativity and chemical reactivity

Quantum chemical calculations are used to determine electronegativity of pure s-, p- and d-states [24]. Considering the chemical hardness, a large HOMO-LUMO gap means a hard molecule and a small HOMO-LUMO gap means a soft molecule. One can also relate the stability of the molecule to hardness, which means that the molecule with low HOMO-LUMO gap means high reactivity. The ionization energy (I) and electron affinity (A) can be obtained as $I = -E_{HOMO}$ and $A = -E_{LUMO}$. Mulliken electronegativity (χ) can be calculated as follows: $\chi = (I + A)/2$ [24]. Softness (S) is a property of molecule that measures the

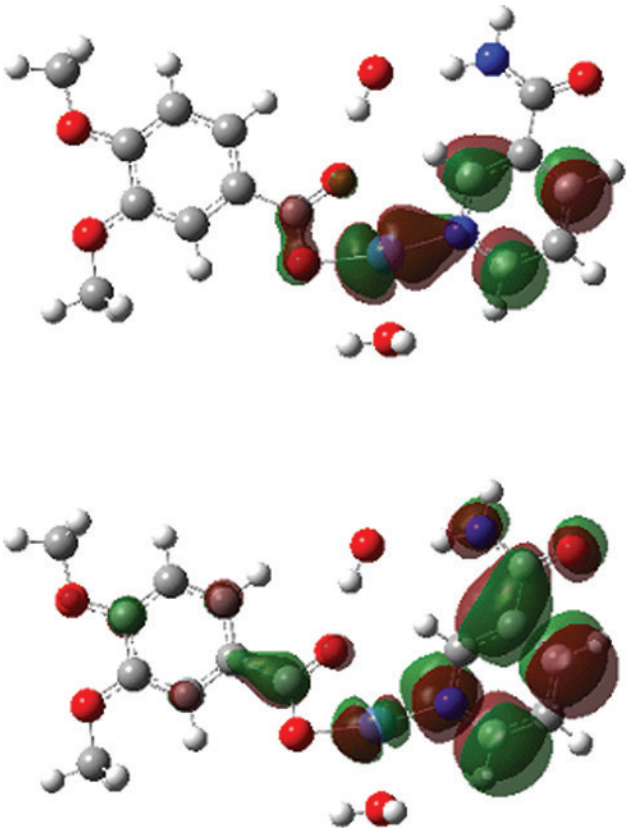

Figure 2 Molecular orbital surfaces and energies for the HOMO and LUMO of the title compound.

extent of chemical reactivity. It is the reciprocal of hardness, $S=1/2\eta$. The hardness (η), in turn, is defined as $\eta=(I\text{-}A)/2$ [25]. The electrophilicity index (ω) is defined as $\omega=(-\chi^2/2\eta)$ and is a measure of energy decrease due to maximal electron flow between donor and acceptor. The values of electronegativity, chemical hardness, softness, and electrophilicity index for the investigated complex in gas phase are 2.629 eV, 1.315 eV, 0.657 eV and –2.628, respectively. The low values of hardness and mulliken electronegativity suggest that the title compound has low chemical reactivity.

Molecular electrostatic potential (MEP)

MEP is related to the electronic density and is a useful descriptor in understanding sites for electrophilic and nucleophilic reactions as well as hydrogen bonding interactions [26, 27]. The value of the molecular electrostatic potential, $V(r)$, for a molecular system at a point of r gives the electrostatic energy on the unit positive charge located at the distance r. The electrostatic potential $V(r)$ is also well suited for analyzing processes based on the "recognition" of one molecule by another, as in drug-receptor, and enzyme-substrate interactions [28, 29]. Experimental $V(r)$ values computed with electron densities obtained from X-ray diffraction data have been used to explore the electrophilicity of hydrogen bonding functional groups [30]. The $V(r)$ values can be determined experimentally by X-ray diffraction or by computational methods [26, 31].

In the present study, the MEP and two dimensional (2D) contour maps drawn in the molecular plane clearly suggest different values of electrostatic potential in the molecule (Figure 3). Negative regions are associated with O1, O5 and O6 with values around –0.521728, –0.492743 and –0.502432 a.u., respectively. It can be suggested that the most preferred regions for electrophilic attack are around O1 and O5. On the other hand, the most maximum positive regions are localized on atoms Ni, C7 and C6 with the values of 0.456214, 0.650145 and 0.544269 a.u., respectively. It can be predicted that the preferred site for a nucleophilic attack is C7. These suggestions of the active

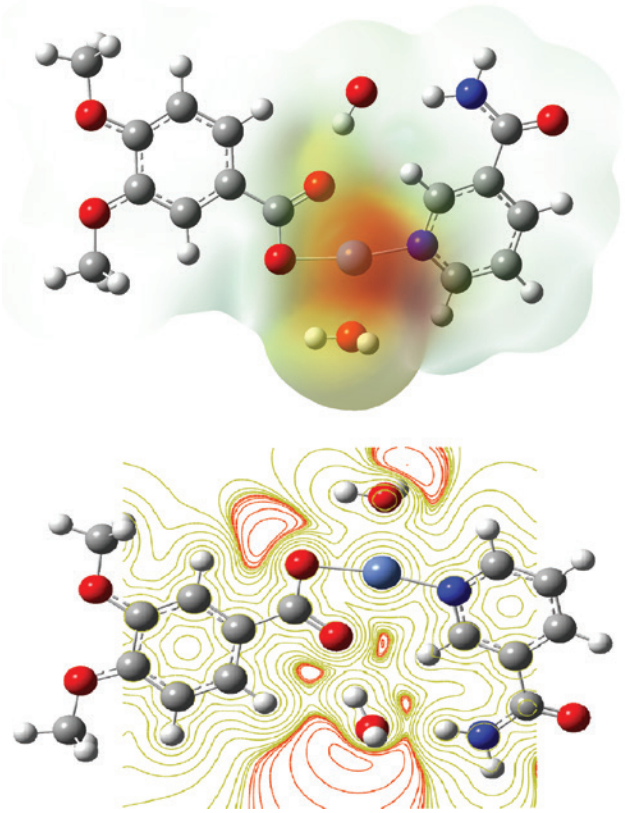

Figure 3 MEP and 2D contour map of the title compound. The maximum positive regions which are preferred sites for a nucleophilic attack are shown in blue; the maximum negative regions which are preferred sites for an electrophilic attack are shown in red.

regions are uniformly supported by Mulliken, NPA and Fukui calculations.

Natural bond orbital (NBO) analysis

NBO analysis is an efficient method for studying intramolecular and intermolecular bonding and interaction among bonds that also provides a convenient basis for investigation of charge transfer or conjugative interactions in molecular systems [32]. Another useful aspect of NBO method is that it gives information about interactions in both filled and virtual orbital spaces, which enhances the analysis of intramolecular and intermolecular interactions.

In this work, the second order Fock matrix analysis was carried out to evaluate the donor-acceptor interactions in the NBO analysis [33]. For each donor NBO (*i*) and acceptor NBO (*j*), the stabilization energy associated with $i \rightarrow j$ delocalization can be estimated by Equation 1, where q_i is the donor orbital occupancy, ε_i, ε_j are diagonal elements

$$E(2) = \Delta E_{ij} = q_i \frac{F(i,j)^2}{\varepsilon_i \varepsilon_j} \tag{1}$$

(orbital energies) and $F(i, j)$ is the off-diagonal NBO Fock matrix clement. In Table S5, the perturbation energies of significant donor-acceptor interactions are presented. The larger the $E(2)$ value, the more intensive is the interaction between electron donors and electron acceptors.

Non-linear optical effects

Molecular materials with non-linear optical (NLO) properties are currently attracting considerable attention because of their potential applications in optoelectronic devices of telecommunications, information storage, optical switching, and signal processing. Recently, various multi-dimensional NLO metal complexes have emerged as candidates for second-order NLO materials because of their potential advantages over one-dimensional (1D) chromophores, such as increasing β responses without undesirable losses of transparency in the visible region and better phase-matching because of their larger off-diagonal components [34]. Metal complexes also display high environmental stability and considerable NLO responses [35–40].

Organometallic and co-ordination chemistry can offer a large variety of molecular and bulk NLO structures in relation to the metal nd configuration, oxidation state, spin state, among other things. The central metal atom of an organometallic complex can readily co-ordinate to conjugated ligands and undergo p-orbital overlap facilitating effective electronic communication which leads to large dipole moment changes between the excited states.

The output from GAUSSIAN03W provides 10 components of the $3\times3\times3$ matrix as β_{xxx}, β_{xxy}, β_{xyy}, β_{yyy}, β_{xxz}, β_{xyz}, β_{yyz}, β_{xzz}, β_{yzz}, β_{zzz}, from which the *x*, *y* and *z* components of β can be calculated as described earlier [41]. When reporting a single value of β, one of the common formats is to simply treat the three independent values for β as a quasi Pythagorean problem which can be solved for the average β by the Equation 2.

$$\beta_{\text{top}} = \sqrt{\beta_x^2 + \beta_y^2 + \beta_z^2} \tag{2}$$

The total static dipole moment μ, the average linear polarizability α, and the first hyperpolarizability β can be calculated by using Equations 3–5, respectively.

$$\mu = \sqrt{(\mu_x^2 + \mu_y^2 + \mu_z^2)} \tag{3}$$

$$\alpha = \frac{1}{3}(\alpha_{xx} + \alpha_{yy} + \alpha_{zz}) \tag{4}$$

$$\beta_{\text{tot}} = [(\beta_{xxx} + \beta_{xyy} + \beta_{xzz})^2 + (\beta_{yyy} + \beta_{yzz} + \beta_{yxx})^2 + (\beta_{zzz} + \beta_{zxx} + \beta_{zyy})^2]^{1/2} \tag{5}$$

The dipole moment, polarizability and the first hyperpolarizability were calculated using ENONLY at the level of B3LYP/6-31G(d) and the results obtained from calculation. The calculated polarizability α and first hyperpolarizability β of I are 39.248 Å^3 and 3.499×10^{-27} cm^5/esu. These values are greater than those of urea (α and β of urea of 3.8312 Å^3 and 0.37289×10^{-30} cm^5/esu), respectively [42].

The polar properties of the title molecule were calculated at the B3LYP/6-31G(d) level using the Gaussian 03W program package. The calculated values of electronic dipole moment μ, polarizability α, and the first hyperpolarizability β for the title compound are 4.659 Debye, 39.248 Å^3 and 3.499×10^{-27} esu, respectively.

Mulliken population and natural population analyses

The Mulliken analysis is the most common population analysis method [43]. In addition, it can also be used to describe the electrostatic potential surfaces [44–46]. In this work, the natural charges were also obtained by NBO analysis [47]; the results are listed in Table S6. It can be

seen that all hydrogen atoms have a net positive charge. The Ni, C6 and C7 atoms bear large positive charges. This is due to the steric interactions. The N1, N2, O1, O2, O3, O4, O5, O6 and O7 atoms contain the most negative charges. The Mulliken net charges are slightly larger than those obtained by the NBO approach.

Fukui function analysis

The Fukui function is among the most basic and commonly used reactivity indicators (Equation 6). It is defined as the change in the density function $\rho(r)$ of the molecule as a consequence of changing the number of electrons N in the molecule, under the constraint of a constant external potential. In this equation, $\rho(r)$ is the electronic density, N is the number of

$$F(r)=\left(\frac{\partial\rho(r)}{\partial N}\right)r \tag{6}$$

electrons and r is the external potential. The Fukui function indicates the propensity of the electronic density to deform at a given position upon accepting or donating electrons [48, 49]. Also, it is possible to define the corresponding condensed or atomic Fukui function on the j_{th} atom site as shown in Equations 7–9.

$$f_j^- = q_j(N) - q_j(N-1) \tag{7}$$

$$f_j^+ = q_j(N+1) - q_j(N) \tag{8}$$

$$f_j^0 = \frac{1}{2}[q_j(N+1) - q_j(N-1)] \tag{9}$$

In these equations, q_j is the atomic charge (evaluated from Mulliken population analysis and electrostatic derived charge) at the j_{th} atomic site in the neutral (N), anionic ($N+1$) or cationic ($N-1$) chemical species. It is important to mention that independent of the approximations used to calculate the Fukui function, the Equation 10 is always followed.

$$\int f(r)dr = 1 \tag{10}$$

The values of the Fukui function were calculated from the NBO charges (Table S7). Note the presence of negative values of the Fukui function. From the calculated values, the reactivity order for the electrophilic attack is O7 > O2 > N2 > O4 > O3 > O1 > N1 > O5. On the other hand, for the nucleophilic attack, the order is Ni > C7 > C1 > C6. Positions of reactive electrophilic sites and nucleophilic sites are in accordance with the total electron density surface and chemical behavior. Calculated values are coherent with regions of the molecular electrostatic potential and Mulliken population charges. The results show that the negative potential sites are on the oxygen atoms and the positive potential sites are around the nitrogen atoms and adjacent carbon atoms.

Conclusions

The compound Ni(II)bis(3,4 dimethoxybenzoate)bis(nicotinamide) dihydrate was characterized by means of X-ray diffraction analysis and IR and UV vis. spectroscopic techniques. The theoretical calculations were performed using DFT method with B3LYP applying 6-31G(d) basis set. The calculated results are in good agreement with experimental data, in spite of the fact that the experimental results belong to solid and liquid phases and theoretical calculations belong to a gaseous phase. The MEP map agrees well with the solid state interactions. Non-linear optical properties of the compound were also investigated. The net charge distribution of the title compound was calculated by using the Mulliken population method and natural population analysis. Molecular orbital coefficient analyses suggest that the electronic spectrum corresponds to $\pi \rightarrow \pi^*$ transitions. In order to understand the electronic transitions of the molecule, TD-DFT calculations on electronic absorption spectra in several solvents and gas phase were performed comparatively. Computational and experimental UV vis. studies for various organic solvents of different polarities indicate that stability of the molecule increases with increase in polarity of the solvent. Solvent effects on intramolecular proton transfer were examined. The compound exhibits good NLO property which is much greater than that of urea. The values of electronegativity, chemical hardness, softness, and electrophilicity index were calculated. Fukui function helps identify the electrophilic and nucleophilic nature of specific sites within the molecule.

Experimental

Synthesis

A mixture of a solution of $NiCl_2 \cdot 6H_2O$ (0.66 g, 2.8 mmol) in H_2O (50 mL), a solution of nicotinamide (0.68 g, 5.6 mmol) in H_2O (10 mL) and a solution of sodium 3,4-dimethoxybenzoate (1.02 g, 5.6 mmol) in H_2O (50 mL) was allowed to stand at room temperature for 10 h, then filtered and set aside at ambient temperature for 1 week, which resulted in crystallization of blue crystals of the nickel complex: mp

148°C–150°C; ^{1}H NMR (200 MHz, $CDCl_3$): δ 8.98 (s, aromatic, 2H), 8.79 (s, aromatic, 2H), 8.19 (d, J=2.5 Hz, aromatic, 4H), 7.61 (dd, J=9.0, 2.5 Hz, aromatic, 2H), 7.56(d, J=2.5 Hz, aromatic, 2H), 7.39 (s, NH_2, 4H), 6.85 (d, J=2.5 Hz, aromatic, 2H), 3.69 (s, O-CH_3, 12 H); ^{13}C NMR (50 MHz, $CDCl_3$): δ 171.3 (CN), 168.2 (CO), 154.7 (C), 152.4 (CH), 149.7 (CH), 149.1 (C), 137.1 (C), 129.8 (C), 127.4 (C), 123.9 (CH), 122.1 (CH), 114.2 (CH), 112.2 (C), 56.8 (OCH), 55.3 (OCH); IR (KBr): 3215, 2243, 1676, 1620, 1515, 1412, 1375, 1271, 1234, 1113, 1022, 766, 686, 653 cm^{-1}; EI-MS: *m/z* 701 [M^++1]. Anal. Calcd for $C_{30}H_{34}N_4NiO_{12}$: C, 51.38; H, 4.89; N, 7.99. Found: C, 51.29; H, 4.81; N, 8.01.

X-ray crystallographic analysis

Diffraction experiments were carried out at 296 K on a Stoe IPDS diffractometer. The structures were solved by direct methods and refined using the programs SHELXS97 and SHELXL97 [50]. All non-hydrogen atoms were refined anisotropically by full-matrix least squares methods [50]. The hydrogen atoms were placed in geometrically idealized positions and refined as riding atoms. Data collection: X-AREA, cell refinement: X-AREA, data reduction: X-RED [51]; program used for molecular graphics: ORTEP-3 for Windows [52]; software used to prepare material for publication: WINGX [53]. Details of crystal data, data collection, structure solution and refinement are listed in Table S1.

Computational procedures

The structural, electronic, and energetic properties of all compounds were computed with the Becke's three-parameter hybrid function [54] combined with the Lee-Yang-Parr correlation, [55] abbreviated as B3LYP, using the 6-31G(d) basis set. In all computations no constraints were imposed on the geometry. Full geometry optimization was performed for each structure using Schlegel's analytical gradient method [25] and the attainment of the energy minimum was verified by calculating the vibrational frequencies that result in absence of imaginary eigen values. All calculations were performed using the GAUSSIAN03 suite of programs [56].

The molecular structure of the title molecule was optimized by the DFT calculations with a hybrid functional B3LYP (Becke's three-parameter hybrid function using the LYP correlation function at 6-31G(d) basis set [57]; all calculations were carried out using Gaussian 03 program package [58]. The vibrational frequencies for optimized molecule were calculated at the same level of the theory and achieved frequencies were scaled by 0.9627 [59]. The electronic absorption spectrum for the optimized molecule was calculated with the time dependent density functional theory (TD-DFT) at B3LYP/6-31G(d) level. In addition, Mulliken population analysis method, FMO, MEP, NLO, Fukui function analysis, NPA and NBO were performed with the same level of theory.

Theoretical UV vis. spectrum of the compound was also obtained by TD-DFT excited state calculation. This calculation is also important in determining the solvent polarity effect and the stability effect. The integral equation formalism of the polarizable continuum (IEF-PCM) [60, 61] model is a useful method to investigate the environmental effects on the compound. The HOMO-LUMO analysis was used to clarify the information regarding charge transfer within the molecule. The HOMO-LUMO energy gap provides important information about stability of the structure and about being a candidate for a non-linear optical material. The polarizability (α), hyperpolarizability (β) and the electric dipole moment were calculated by using the B3LYP/6-31G(d,p) approach. The redistribution of electron density in various bonding, antibonding orbitals and $E(2)$ (energy difference between donor and acceptor natural bond orbitals) energies were calculated by natural bond orbital (NBO) [62] analysis to give clear evidence of stabilization originating from the hyperconjugation of various intramolecular interactions.

Molecular electrostatic potential (MEP) analysis can be used to find the reactive sites of the compounds. The electrostatic potential contour map is related to electrophilic and nucleophilic reactivities. In this paper, the net charges were calculated with Mulliken population method and natural population analysis (NPA). The calculated natural atomic charge values from the natural population analysis procedures were obtained from NBO analysis. The individual atomic charges calculated by Mulliken population analysis were used.

Online supplementary data

Tables S1–S7 of Supplementary Material to this paper contain the molecular characterization, X-ray crystallographic analysis and computational results of the title complex. Additional characterization of the compound has been deposited in the Cambridge Crystallographic Data Centre, file CCDC 931589. These data can be obtained free of charge via www.ccdc.cam.ac.uk/data_request/cif, by emailing data_request@ccdc.cam.ac.uk, or by contacting Cambridge Crystallographic Data Centre, 12, Union Road, Cambridge CB2 1EZ, UK; fax: +44-1223-336033.

Acknowledgment: The authors wish to acknowledge the Faculty of Arts and Sciences, Ondokuz Mayis University, Turkey, for the use of the STOE IPDS 2 diffractometer (purchased under grant F.279 of the University Research Fund). This study was financed by Gümüşhane University (BAP) (Project no: 13.B0110.02.3) for (E.Ç.K.).

References

[1] Miwa, Y.; Mizuno, T.; Tsuchida, K.; Taga, T.; Iwata, Y. Experimental charge density and electrostatic potential in nicotinamide. *Acta Crystallogr. Sect. B* **1999**, *55*, 78–84.

[2] Aakeröy, C. B.; Beatty, A. M. Supramolecular assembly of low-dimensional silver(I) architectures *via* amide-amide hydrogen bonds. *Chem. Commun*. **1998**, *10*, 1067–1068.

[3] Yarks, J.; He, L.; Adams, J. D. Early administration of nicotinamide prevents learning and memory impairment in mice induced by 1-methyl-4-phenyl-1,2,3,6-tetrahydropyridine. *J. Pharmacol. Biochem. Behav*. **2004**, *78*, 179–183.

[4] Mycek, M. J.; Harvey, R. A.; Champe, P. C. ed. Lippincott's Illustrated Reviews: Pharmacology, 2nd ed; Lippincott-Raven: Philadelphia, PA,1997.

[5] Zachariadis, P.; Hadjikakou, S.; Hadjiliadis, N.; Michaelides, A.; Skoulika, S.; Ming, Y.; Xiaolin, Y. Synthesis, study and structural characterization of a new water soluble hexanuclear silver(I) cluster with the 2-mercapto-nicotinic acid with possible antiviral activity. *Inorg. Chim. Acta* **2003**, *343*, 361–365.
[6] Chohan, Z.; Rauf, A.; Noreen, S.; Scozzafava, A.; Supuran, C. Antibacterial Cobalt (II), Nickel (II) and Zinc (II) Complexes of Nicotinic Acid derived Schiff-bases. *J. Enzyme Inhib. Med. Chem.* **2002**, *17*, 101–106.
[7] Kaya, A. A.; Çelenk, Kaya E.; Öztürk Sarıkaya, S. B.; Onaran, A. Synthesis, antifungal activity and carbonic anhydrase inhibitory properties of Cu(II)bis(3,4-dimethoxybenzoate) bis(nicotinamide) dihydrate. *Curr. Enzym. Inhib.* **2015**, *11*, 32–38.
[8] Chernyavskaya, A. A.; Loginova, N. V.; Polozov, G. I.; Shadyro, O. I.; Sheryakov, A. A.; Bondarenko, E. V. Synthesis and antimicrobial activity of silver(I) and copper(II) complexes with 2-(4,6-di-*tert*-butyl-2,3-dihydroxyphenylsulfanyl)acetic acid. *Pharm. Chem. J.* **2006**, *40*, 413–415.
[9] Singh, K.; Barwa, M. S.; Tyagi, P. Synthesis, characterization and biological studies of Co (II), Ni (II), Cu (II) and Zn (II) complexes with bidentate Schiff bases derived from heterocyclic ketone. *Eur. J. Med. Chem.* **2006**, *41*, 147–153.
[10] Phaniband, M. A.; Dhumwad, S. D. Synthesis, characterization and biological studies of Co II, Ni II, Cu II and Zn II complexes of Schiff bases derived from 4-substituted carbostyril-[quinolin-2(1*H*)-one]. *Transit. Met. Chem*. **2007**, *32*, 1117–1125.
[11] Yu, L. C.; Lai, L.; Xia, R.; Liu, S. L. Syntheses and crystal structures of Zn(II) and Co(II) complexes with ofloxacin and enoxacin. *J. Coord. Chem*. **2009**, *62*, 1313–1319.
[12] Coogan, T. P.; Latta, D. M.; Snow, E. T.; Costa, M. Toxicity and Carcinogenicity of Nickel Compounds. In *Critical Reviews in Toxicology*. CRC Press: Boca Raton, FL, 1989.
[13] ATSDR (Agency for Toxic Substances and Disease Registry). 1988. Toxicological Profile for Nickel, ATSDR/U.S. Public Health Service, ATSDR/TP-88/19.
[14] Çelenk, K. E.; Demircioğlu, Z.; Kaya, A. A.; Büyükgüngör O. Synthesis, X-ray structural characterization, NLO, MEP, NBO and HOMO-LUMO analysis using DFT study of Co(II)bis(3,4 dimethoxybenzoate)bis(nicotinamide) dihydrate. *Mol. Cryst. Liq. Cryst.* **2015**, *609*, 103–117.
[15] Kaya, A. A.; Demircioğlu, Z.; Celenk, E.; Büyükgüngör, O. Synthesis, X-ray structural characterization, NLO, MEP, NBO and HOMO-LUMO analysis using DFT study of Zn(II)bis(3,4 dimethoxybenzoate) bis(nicotinamide) dihydrate. *Heterocycl. Commun.* **2014**, *20*, 51–59.
[16] Köse, D. A.; Kaya, A.; Necefoğlu, H. Synthesis and characterization of Bis(N,N-diethylnicotinamide) *m*-hydroxybenzoate complexes of Co(II), Ni(H), Cu(II), and Zn(II). *Rus. J. Coord. Chem.* **2007**, *33*, 422–427.
[17] Chemia, D. S.; Zyss, J. Non-linear Optical Properties of Organic Molecules and Crystal. Academic Press: New York, 1987.
[18] Karpagam, J.; Sundaraganesan, N.; Sebastian, S.; Manoharan, S.; Kurt, M. Molecular structure, vibrational spectroscopic, first-order hyperpolarizability and HOMO, LUMO studies of 3-hydroxy-2-naphthoic acid hydrazide. *J. Raman Spectrosc.* **2010**, *41*, 53–62.
[19] Fleming, I. Frontier Orbitals and Organic Chemical Reactions, Wiley: London, 1976.
[20] Fukui, K. Theory of Orientation and Stereo Selection; Springer-Verlag: Berlin, 1975.
[21] Hohenberg, P.; Kohn, W. Inhomogeneous electron gas. *Phys. Rev*. **1964**, *136*, 864–871.
[22] Kim, K. H.; Han, Y. K.; Jung, J. Basis set effects on relative energies and HOMO-LUMO energy gaps of fullerene C-36. *Theo. Chem. Acc.* **2005**, *113*, 233–237.
[23] Aihara, J. Weighted HOMO-LUMO energy separation as an index of kinetic stability for fullerenes. *Theo. Chem. Acc*. **1999**, *102*, 134-138.
[24] Avvakumov, E.; Senna, M.; Kosova, N. Soft Mechanochemical Synthesis a Basis for New Chemical Technologies; Kluwer Academic Publishers: New York, Boston, Dordrecht, London, Moscow, 2002
[25] Allen F. H.; Kennard O.; Watson D. G.; Brammer L.; Orpen A. G. Tables of bond lengths determined by X-ray and neutron diffraction. Part 1. Bond lengths in organic compounds. *J. Chem. Soc. Perkin Trans. 2* **1987**, *1*, 1–19.
[26] Grabowski, S. J.; Leszczynski, J. Unrevealing the Nature of Hydrogen Bonds: π –Electron Delocalization Shapes H-Bond Features. in: Hydrogen Bonding - New Insights. Grabowski, J. S. Kluwer, Academic Publishers: New York, 2006, 491–495.
[27] Tomasi, J.; Mennucci, B.; Cammi, R. Quantum mechanical continuum solvation models. *Chem. Rev.* **2005**, *105*, 2999–3093.
[28] Scrocco, E.; Tomasi, J. Electronic molecular structure, reactivity and intermolecular forces: an euristic interpretation by means of electrostatic molecular potentials. *Adv. Quantum Chem.* **1978**, *11*, 115–193.
[29] Luque, F. J.; Lopez, J. M.; Orozco, M. Perspective on electrostatic interactions of a solute with a continuum. A direct utilization of ab initio molecular potentials for the prevision of solvent effects. *Theor. Chem. Acc*. **2000**, *103*, 343–345.
[30] Politzer, P.; Laurence, P. R.; Jayasuriya K.; McKinney J. Molecular electrostatic potentials: an effective tool for the elucidation of biochemical phenomena. *Special issue of Environ. Health Perspect* **1985**, *61*, 191–202.
[31] Scrocco, E.; Tomasi, J. Topics in Current Chemistry, Vol. 7. Springer Verlag, Berlin, 1973.
[32] Snehalatha, M.; Kumar, C. R.; Joe, I. H.; Sekar, N.; Jayakumar, V. S. Spectroscopic analysis and DFT calculations of a food additive carmoisine. *Spectrochim. Acta A*, **2009**, *72*, 654–662.
[33] Szafran, M.; Komasa, A.; Adamska, E. B. Crystal and molecular structure of 4-carboxypiperidinium chloride (4-piperidinecarboxylic acid hydrochloride). *J. Mol. Struct.* **2007**, *827*, 101–107.
[34] Coe, B. J.; Harris, J. A.; Jones, L. A.; Brunschwig, B. S.; Song, K.; Clays, K.; Garin, J.; Orduna, J.; Coles, S. J.; Hursthouse, M. B. Syntheses and properties of two-dimensional charged nonlinear optical chromophores incorporating redox-switchable *cis*-tetraammineruthenium(II) centers. *J. Am. Chem. Soc*. **2005**, 127, 4845–4859.
[35] Kanis, D. R.; Ratner, M. A.; Marks, T. J. Design and construction of molecular assemblies with large 2nd-order optical nonlinearities – quantum-chemical aspects. *Chem. Rev*. **1994**, *94*, 195–242.
[36] Bella, S. D. Second-order nonlinear optical properties of transition metal complexes. *Chem. Soc. Rev*. **2001**, *30*, 355–366.
[37] Lacroix, P. G. Second-order optical nonlinearities in coordination chemistry: the case of bis(salicylaldiminato)metal schiff base complexes. *Eur. J. Inorg. Chem*. **2001**, 339–348.

[38] Long, N. J. Organometallic compounds for nonlinear optics – the search for En-light-enment. *Angew. Chem., Int. Ed. Engl*. **1995**, *34*, 21–38.
[39] Costes, J. P.; Lamere, J. F.; Lepetit, C.; Lacroix, P. G.; Dahan, F. New second-order NLO materials based on polymeric borate clusters and GeO4 tetrahedra: a combined experimental and theoretical study. *Inorg. Chem*. **2005**, *44*, 1973–1982.
[40] Coe, B. J.; Harris, J. A.; Brunschwig, B. S.; Asselberghs, I.; Clays, K.; Garin, J.; Orduna, J. Three-dimensional non linear optical chromophores based on;metal-to-ligand charge-transfer from ruthenium(II) or iron(II) centers. *J. Am. Chem. Soc*. **2005**, *127*, 13399–13410.
[41] Karaer, H.; Gümrükçüoğlu, I. E. Synthesis and spectral characterisation of novel azo-axomethine dyes. *Turk. J. Chem*. **1999**, *23*, 67–71.
[42] Sun, Y. X.; Hao, Q. L.; Wei, W. X.; Yu, Z. X.; Lu, L. D.; Wang, X.; Wang, Y. S. Experimental and density functional studies on 4-(3,4-dihydroxybenzylideneamino)antipyrine, and 4-(2,3,4-trihydroxybenzylideneamino)antipyrine. *J. Mol. Struct*. (*theochem*) **2009**, *904*, 74–82.
[43] Sidir, I.; Sidir, Y. G.; Kumalar, M.; Tasal, E. Ab initio Hartree-Fock and density functional theory investigations on the conformational stability, molecular structure and vibrational spectra of 7-acetoxy-6-(2,3-dibromopropyl)-4,8-dimethylcoumarin molecule. *J. Mol. Struct*. **2010**, *964*, 134–151.
[44] Balachandran,V.; Parimala, K. Tautomeric purine forms of 2-amino-6-chloropurine (N_9H_{10} and N_7H_{10}): Structures, vibrational assignments, NBO analysis, hyperpolarizability, HOMO-LUMO study using B3 based density functional calculations. *Spectrochim. Acta A* **2012**, *96*, 340–351.
[45] Lakshmi, A.; Balachandran, V. Rotational isomers, NBO and spectral analyses of N-(2-hydroxyethyl) phthalimide based on quantum chemical calculations. *J. Mol. Struct*. **2013**, *1033*, 40–50.
[46] Ramalingama, S.; Karabacak, M.; Periandy, S.; Puviarasan, N.; Tanuja, D. Spectroscopic (infrared, Raman, UV and NMR) analysis, Gaussian hybrid computational investigation (MEP maps/HOMO and LUMO) on cyclohexanone oxime. *Spectrochim. Acta A* **2012**, *96* 207–212.
[47] Mulliken, R. S. Electronic population analysis on LCAO–MO molecular wave functions. *J. Chem. Phys*. **1955**, *23*, 1833–1840.
[48] Parr, R. G.; Yang, W. Functional Theory of Atoms and Molecules; Oxford University Press: New York; 1989.
[49] Ayers P. W.; Parr R. G. Variational principles for describing chemical reactions: the fukui function and chemical hardness revisited. *J. Am. Chem. Soc*. **2000**, *124*, 2010–2018.
[50] Sheldrick, G. M. SHELXS-97 and Sheldrick G.M., SHELXL-97. Program for Crystal Structures Refinement, University of Gottingen, Gottingen, 1997.
[51] Stoe & Cie, X-AREA (Version 1.18) and X-RED32 (Version 1.04) Stoe & Cie, Darmstadt, 2002.
[52] Farrugia L. J. *WinGX* suite for small-molecule single-crystal crystallography. *J. Appl. Crystallogr*. **1997**, *30*, 565–566.
[53] Farrugia L. J. *WinGX* suite for small-molecule single-crystal crystallography. *J. Appl. Crystallogr*., **1999**, *30*, 837-838.
[54] Stephens P. J.; Devlin F. J.; Chabalowski C. F.; Frisch M. J. Ab initio calculation of vibrational absorption and circular dichroism spectra using density functional force fields. *J. Phys. Chem*. **1994**, *98*, 11623–11627.
[55] Odabaşoğlu M.; Albayrak Ç.; Büyükgüngör O.; Goesmann H. 4-[(3-Chlorophenyl)diazenyl]-2-{[tris(hydroxymethyl)methyl] aminomethylene}-cyclohexa-3,5-dien-1(2*H*)-one. *Acta Crystallographica* C59 **2003**, *59*, o234–o236.
[56] Frisch, M. J.; Trucks, G. W.; Schlegel, H. B.; Scuseria, G. E.; Robb, M. A.; Cheeseman, J. R.; Montgomery, J. A.; Vreven, T. J.; Kudin, K. N.; Burant, J. C.; et al. Gaussian 03, Revision E.01, Gaussian, Inc., Pittsburgh, PA, 2003.
[57] Loudon, M. G. Study Guide and Solutions Manual to Accompany Organic Chemistry; 4th edition; Roberts & Company Publishers: Oxford, USA, 2002.
[58] Bondi, A. J. van der Waals Volumes and Radii. *Phys. Chem*. **1964**, 68, 441–451.
[59] Albayrak, Ç.; Gümrükçüoğlu, I. E.; Odabaşoğlu, M.; Iskeleli, N. O.; Ağar, E. Synthesis, spectroscopic, and molecular structure characterizations of some azo derivatives of 2-hydroxyacetophenone. *J. Mol. Struct*. **2009**, *932*, 43–54.
[60] Miertus, S.; Scrocco, E.; Tomasi J. Electrostatic interaction of a solute with a continuum. a direct utilization of ab initio molecular potentials for the prevision of solvent effects. *Chem. Phys*. **1981**, *55*, 117–129.
[61] Cossi, M.; Rega, N.; Scalmani, G.; Barone, V. Energies, structures, and electronic properties of molecules in solution with the C-PCM solvation model. *J. Comput. Chem*. **2003**, *24*, 669–681.
[62] Keresztury, G.; Holly, S.; Varga, J.; Besenyei, G.; Wang, AV.; Durig, J. R. Vibrational spectra of monothiocarbamates-II. IR and Raman spectra, vibrational assignment, conformational analysis and *ab initio* calculations of *S*-methyl-*N,N*-dimethylthiocarbamate. *Spectrochim. Acta A* **1993**, *49*, 2007–2017.

Supplemental Material: The online version of this article (DOI: 10.1515/hc-2016-0099) offers supplementary material, available to authorized users.